
DaBiT: Depth and Blur informed Transformer for Joint Refocusing and Super-Resolution

Crispian Morris

Department of Computer Science
University of Bristol
Bristol, UK
crispian.morris@bristol.ac.uk

Nantheera Anantrasirichai

Department of Computer Science
University of Bristol
Bristol, UK
n.anantrasirichai@bristol.ac.uk

Fan Zhang

Department of Computer Science
University of Bristol
Bristol, UK
fan.zhang@bristol.ac.uk

David Bull

Department of Computer Science
University of Bristol
Bristol, UK
dave.bull@bristol.ac.uk

Abstract

In many real-world scenarios, recorded videos suffer from accidental focus blur, and while video deblurring methods exist, most specifically target motion blur. This paper introduces a framework optimised for the joint task of *focal* deblurring (refocusing) and video super-resolution (VSR). The proposed method employs novel map guided transformers, in addition to image propagation, to effectively leverage the continuous spatial variance of focal blur and restore the footage. We also introduce a flow re-focusing module to efficiently align relevant features between the blurry and sharp domains. Additionally, we propose a novel technique for generating synthetic focal blur data, broadening the model’s learning capabilities to include a wider array of content. We have made a new benchmark dataset, DAVIS-Blur, available. This dataset, a modified extension of the popular DAVIS video segmentation set, provides realistic out-of-focus blur degradations as well as the corresponding blur maps. Comprehensive experiments on DAVIS-Blur demonstrate the superiority of our approach. We achieve state-of-the-art results with an average PSNR performance over 1.9dB greater than comparable existing video restoration methods. Our source code will be made available at <https://github.com/crispianm/DaBiT>

1 Introduction

Videos captured in challenging circumstances, such as low light, or by less experienced shooters may exhibit blurriness, including motion blur and out-of-focus blur. Consequently, a deblurring process is necessary to enhance visual quality. However, this remains a challenging task, even for modern deep learning models, because of the rapid loss of information as the blur intensifies.

While traditional methods employ deconvolution-based algorithms in order to sharpen input images, advances in deep learning techniques have enabled direct learning of a mapping from blurry to sharp. Recent contributions in this field, particularly those using convolutional neural networks (CNNs), have significantly improved upon the deconvolution-based algorithms, as demonstrated by image-based contributions such as DeBlurGAN [21], NAFNet [6], and BIPNet [12]. However, a significant challenge still exists in the form of video content; while these methods may produce

visually pleasing results for individual frames, they often introduce temporal inconsistencies when applied to a video sequence.

One explanation for this is that CNNs can struggle to capture long-range dependencies within video sequences; these are highly beneficial for handling complex image degradations like blur while retaining high-frequency details. The transformer architecture [11] has emerged as a promising alternative for various computer vision tasks, due largely to its self-attention mechanism. The transformer’s ability to learn these global dependencies and accurately model long-range interactions makes it particularly well-suited for video deblurring, due to the inherent temporal dependencies of blur, as demonstrated by [25, 26]. While these methods are well-suited to removing camera shake and motion blur, scenarios exist where motion blur is desirable, and where errors in autofocus or camera operation also cause segments of the video to be out-of-focus unintentionally. In such cases, focal points will vary dynamically with the content, obscuring a large area of frames in the sequence. The spatio-temporal variance inherent in this effect makes the out-of-focus blur problem significantly more challenging to resolve than ‘simple’ motion blur. Motivated by this, we introduce a Depth and Blur informed Transformer (DaBiT), which aims to learn the mapping from blurry to focused, employing pseudo ground truth blur and depth maps for inference.

The main contributions of this work are as follows:

- The introduction of DaBiT, a novel transformer-based architecture integrating depth and blur maps, addressing the challenge of video defocus deblurring.
- The adoption of a novel video inpainting approach to deblurring, focusing the model on out-of-focus sections.
- The development of a novel synthetic blur generation process for realistic training data.
- The integration of a video super-resolution component to handle high resolution content efficiently, enhancing the model’s performance.

2 Related Work

Video Deblurring. Deblurring aims to remove blur caused by incorrect focus, object motion, or camera shake from input videos. It can be accomplished either as individual images [44, 1, 20, 37, 45] or as sequences of images [15, 16, 48, 18, 26, 25]. Importantly, only a handful of the *individual image* works aim to remove blur caused by incorrect focus [1, 34, 32, 45, 47, 9, 7].

When methods trained to deblur individual images are applied to videos, temporal inconsistencies are prone to appear, due to small errors and inconsistencies in each image being restored differently. This necessitates the creation of specific network architectures for video deblurring. Recently, Zhong *et al.* proposed a Blur Interpolation Transformer [48] based on Swin transformer blocks, that achieved competitive performance for motion deblurring. Shang *et al.* attempted the joint task of frame interpolation and motion deblurring with VIDUE [33], improving temporal consistency significantly for the challenging $16\times$ interpolation task. To our knowledge, no work exists aiming to remove focal blur from entire video sequences.

Video Super-Resolution. Video Super-Resolution (VSR) is a well studied task, with many significant recent research contributions. VSR is however challenging when compared to image super-resolution: not only by virtue of higher computational requirements, but also due to the challenge of maintaining temporal consistency across frames. In order to remedy this, two primary approaches have been proposed: sliding window-based and recurrent-based methods. While sliding window-based VSR methods [17, 23, 36, 22] estimate the upscaled frames using adjacent frames in the pixel space, recurrent-based methods [14, 27, 4, 5] propagate latent features sequentially to synthesise the HR target frame.

No specific model architecture has yet dominated, and a variety of different model backbones have been utilised for this task. In 2023, Zhou *et al.* proposed Upscale-A-Video [50] introducing the concept of using text-guided diffusion for video upscaling, achieving a high perceptual quality. Most recently, Xu *et al.* proposed VideoGigaGAN [41], balancing the inherent conflict of preserving high-frequency details whilst maintaining temporal consistency using their high-frequency shuffle component.

3 Synthetic Blurred Video Generation

Deep learning necessitates a substantial volume of data to train the model effectively. While unsupervised learning techniques exist, supervised learning-based methods still outperform them in terms of both accuracy and speed. However, obtaining paired datasets of blurred and clean sequences is time-consuming and content diversity can be limited. Hence, we introduce a new approach to generate synthetic datasets, and use it to create DAVIS-Blur, a modified version of the DAVIS [30] video segmentation test set.

3.1 Focal Blur Simulation

In order for our model to learn the nature of focal blur, an accurate blur model is required.

We begin with an input video $I_{in} = \{I_t \in \mathbb{R}^{3 \times H \times W}\}_{t=1}^T$ with T frames. We then compute the depth maps $D = \{D_t \in \mathbb{R}^{1 \times H \times W}\}_{t=1}^T$ for the input using DepthAnything [42], due to its ability to predict temporally consistent depths at a level surpassing other state-of-the-art models such as MiDaS [31] or ZoeDepth [3]. Using the depth maps, the spatial variance of focal blur is able to be modelled. We begin by setting the focal point at a depth f , and defining a focal range f_r centred on the focal point.

We then apply gaussian blur kernels $G(x, y) = \frac{1}{2\pi\sigma^2} e^{-\frac{x^2+y^2}{2\sigma^2}}$, with $\sigma = 5$, to the image in both directions along its depth axis, scaling symmetrically from zero inside the focal range to a maximum kernel size of $n_{max} \times n_{max}$. In this way, we blur the furthest depths from the focal point the most, creating a realistic focal blur effect.

During training, a random frame sequence from I_{in} of length $l, l < T$ is taken, along with r random global reference frames from elsewhere in the video. A random focal point (f) and focal range (f_r) are selected, along with a random focus rate $\frac{df}{dt}$, dictating the velocity at which the focal point will change in the sequence. A random maximum blur kernel size $n_{max} \in \{x \in \mathbb{Z} : 3 \leq x \leq 11, x \text{ is odd}\}$ is chosen, and the sequence and its global reference frames are blurred in a temporally variant manner, denoted as \widetilde{I}_{in} , simulating a focus shift. The spatial blur intensity information is recorded and used to create a ground truth blur map $B = \{B_t \in \mathbb{R}^{1 \times H \times W}\}_{t=1}^T$, assisting our model during training. We also introduce data augmentation by means of a random horizontal flip and random reversal of sequence during the training. Finally, to enable super-resolution, we downsample the blurred sequence, along with its blur and depth maps, denoted as $\widetilde{I}_{lr}, B_{lr},$ and D_{lr} , respectively. Further details of this approach are provided in the supplementary material.

The variation in blur intensity and focus speed simulates a broad range of focus shifts. Some are representative of sequences which do not contain any additional global information (e.g. $\frac{df}{dt} = 0$, so l is out-of-focus in the same spatio-temporal regions), and some which contain enough focused footage to be able to nearly reconstruct the whole sequence using only image propagation (e.g. f is varied completely across $\min(D)$ and $\max(D)$). This allows a given model to learn to deblur fully out-of-focus frames while not discarding the information contained in focused frames.

For creating our test set, we set $l = T, n_{max} = 7, f_r = 100$, and fix the initial focal point $f = 0$ for all 50 sequences in the DAVIS [30] test set. The focus rate is then set at $\max(D)/l$, according to each sequence’s length. This simulates a complete focus shift from near to far, across the full length of the sequence. The large range of sequence lengths in the DAVIS set allow a wide range of focus shifts to be synthesised, thus posing a challenging task. The resulting new dataset, DAVIS-Blur, is released as a part of this work.

4 Methodology

The proposed DaBiT framework is shown in Figure 1. The frames and pre-computed inputs to both the model and the flow restoration module are downsampled to allow footage of high resolution to be processed faster, also adding flexibility in other use cases, such as video editing.

Given a low-resolution, blurry input video I_{lr} with T frames and corresponding blur and depth maps B_{lr} and D_{lr} , our aim is to remove the focal blur in a spatio-temporally consistent manner and jointly upscale the video to high resolution. During inference, the blur maps can be estimated using a combination of the depth maps and a wavelet transform. By taking high-frequency regions of the frame found with the transform as regions of focus, we take the sum of the wavelet components

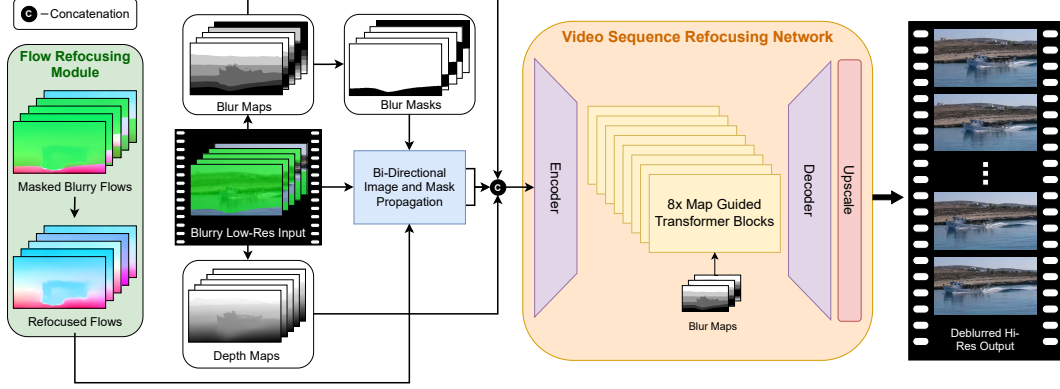


Figure 1: The architecture of the DaBiT model.

for each depth, and use the inverse of this as a map of the blurred regions. These maps are needed to employ our inpainting-based approach to this task, under the assumption that there are other spatio-temporally aligned regions in the video which exhibit less or no blur. This takes the form of integrating blur *masks*, allowing our model to identify the regions of focus in a given input, and it reduces the difficulty of the task greatly.

To generate the blur mask sequence $M = \{M_t \in \mathbb{R}^{1 \times H \times W}\}_{t=1}^T$, we begin with the blur map sequence B_{lr} , where the intensity of the grayscale image corresponds to the amount of blur present in the spatial region. The maps are binarised by setting all but the lowest value equal to one, trivially distinguishing regions of focus from those containing blur, and delivering the resulting masks, M_{lr} . Separately, we also employ RAFT [35] to estimate the blurry input frames' flows, $\tilde{F} = \{\tilde{F}_t \in \mathbb{R}^{2 \times H \times W}\}_{t=1}^{T-1}$. The flows are passed to the refocusing module (subsection 4.1) to obtain in-focus flows F_{lr} . After refocusing, \tilde{I}_{lr} and M_{lr} are passed to a non-learnable image propagation module [49], which warps flows F to recover details present at different times in the sequence, using forward and backward consistency error [13, 40]. It returns updated input frames \tilde{I}'_{lr} as well as the corresponding updated masks M'_{lr} , dilating the spatio-temporal focused area. The blur maps are left unaltered in the event that propagation delivers blurred or temporally inaccurate content.

\tilde{I}'_{lr} , M'_{lr} , D_{lr} , and B_{lr} are then passed to an encoder, which compresses the inputs into a latent representation, enabling a significant reduction in compute for the map guided transformers. Next, the latent features are passed into the map-guided sparse transformer blocks, processed, and decoded into frames. Finally, the deblurred frames are passed to an upscaler, which achieves $2 \times$ super-resolution, returning J_{out} . While the potential is not limited, upscaling was only tested to $2 \times$ due to memory constraints.

The specifics of each component are detailed below.

4.1 Flow Refocusing Module

In order for the image propagation to be most effective, optical flows are required to be as close to ground truth as possible. Similarly to ProPainter [49], which employs a pre-trained recurrent flow completion network for inpainting objects from flows, we design a pre-trained network for aiding in the refocusing of flows. During inference, the optical flows estimated by RAFT [35] are between blurry, low-resolution frames. Errors in the flow have the potential to propagate into the reconstructed footage as artefacts and temporal inconsistencies. To reduce the likelihood of this, we train a separate network specifically to refocus the degraded flow, due to the distinct difference in task between refocusing flows and refocusing video sequences. We follow previous works [4, 5, 49] in choosing a recurrent network architecture, due to its efficiency and performance relative to a sliding window approach.

The architecture of this module can be seen in Figure 2. During training, we create samples in the same manner detailed in subsection 3.1, and use binarised blur maps as masks for the flows. We

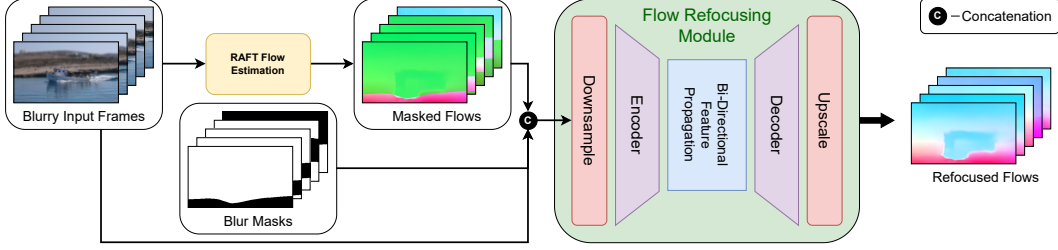


Figure 2: The architecture of the Flow Refocusing module.

downsample the inputs by a factor of eight for increased speed, and pass the masked flows, binary masks, and blurry frames to an encoder. Following [5], we perform deformable alignment based on deformable convolution [10, 51], propagating in-focus regions from other flows and lessening the burden of refocusing of the module. We then decode the features into refocused flows, which are used in the image propagation module to reduce the burden on the transformer.

4.2 DaBiT

Transformers are undoubtedly an excellent tool for video restoration, but their high memory footprint and slow inference speed poses problems in many use cases. The novel sparse transformer blocks proposed by Zhou *et al.* [49] partially overcome this issue by building on the window-based transformer blocks proposed in E^2 FGVI [24] and FGT [46]. Hence, we adopt a similar architecture to that of ProPainter, but with a few modifications. Firstly, in addition to the input frames and binary masks, we encode the depth and blur maps. This enables the transformer to learn the spatial relation between blur and depth, and ensures high similarity by encouraging consistent depth across frames. We encode this fused input into the feature space in order to further speed up processing. In contrast to ProPainter, a learnable feature propagation module is not employed before the transformer due to the minimal performance loss when ablated.

We then use soft split [28] to generate patch embeddings P , and decompose them into $m \times n$ non-overlapping windows of dimension $h \times w$. This results in P_{win} , which we obtain the query, key, and value matrices from. Following [49], we design separate strategies for the query and key/value spaces as described below. We also integrate global tokens [46] and the window expand strategy [28] in order to replicate the efficient 5×9 window size.

Query Space. Since we are in effect attempting to inpaint a very large mask (up to 100% of the frame), sparsity will not always result in as large a performance saving. However, we hypothesise that communicating to the model the areas which are more or less blurry, and how blurry those regions are, will aid the transformer’s self-attention mechanism. However, savings are still possible from any regions not exhibiting blur. To this end, we downsample the blur maps and apply MaxPooling across frames to obtain a query mask M_Q , which is zero at a pixel (x, y) if the frames in question are all in focus at that point. The mask additionally communicates which areas of the frames are most blurred, assisting the attention mechanism by effectively acting as a form of positional encoding for each patch.

Key and Value Space. We employ the same strategy as [49], and incorporate a temporal stride of two, effectively dividing computation of frames evenly between each of the eight transformer blocks. This is primarily motivated by the relative similarity of defocus between two given frames, and the 50% compute savings during training and inference associated with it.

Super Resolution. Finally, we add an additional upsampling module inspired by [5] consisting of multiple cascading PixelShuffle layers to achieve $2 \times$ video super-resolution. This component allows for flexibility in input resolution without unnecessarily increasing model size or speed.

4.3 Loss functions

We define three loss terms for training our model. The first is the Charbonnier loss between the model’s predicted HR frames and the ground truth HR frames,

$$\mathcal{L}_{Charb}(I_{pred}, I_{gt}) = \sqrt{(I_{pred} - I_{gt})^2 + \epsilon^2}, \quad (1)$$

where I_{pred} and I_{gt} are the predicted frames and the ground-truths, respectively, and $\epsilon = 0.001$. The second loss term denotes the l_1 loss between only the blurred areas of the input frames and the corresponding regions in the ground truth frames. The third term is the inverse of the second, comparing the focused input regions to the focused ground truth regions. These two loss terms are inspired by various inpainting approaches, and encourages the model to remove blur while remaining true to the in-focus regions. Thus, in total, the loss is expressed as

$$\mathcal{L}_{tot} = \alpha \mathcal{L}_{Charb}(I_{pred}, I_{gt}) + \beta l_1(\hat{I}_{pred}, \hat{I}_{gt}) + \gamma l_1(\tilde{I}_{pred}, \tilde{I}_{gt}), \quad (2)$$

where \hat{I} denotes only the blurred regions of the frame sequences, and \tilde{I} denotes only the focused regions. Both of two the l_1 loss term inputs are resized to the input resolution, enabling the model to be more sensitive to the numerically small values of the Charbonnier super-resolution loss term. For training, we set $\alpha = \beta = \gamma = 1$.

5 Experiments

Training Details and Metrics. We train our models on both the Youtube-VOS [39] and BVI-DVC [29] datasets. During the training of the Flow Refocusing module, 20 iterations of RAFT [35] are used for flow estimation with a frame sequence length of 10. We follow [49] and apply propagation to $8\times$ downsampled feature vectors. In the main model, eight sparse transformer blocks with four heads are employed for deblurring a local video sequence $l = 10$, with $r = 6$ reference frames. The map guided transformer window size is 5×9 , and the extended size is half of the window size. We train both DaBiT and the Flow Refocusing module using the Adam optimiser [19] with a batch size of 1 on frames of size 432×240 , due to memory constraints. We fix the learning rate at 10^{-4} , and train the Flow Refocusing module for 100k iterations and DaBiT for 300k iterations on a single NVIDIA RTX 4090 GPU. Following [43], we use PSNR and SSIM [38] to evaluate our methods, as well as tOF [8] for measuring temporal consistency.

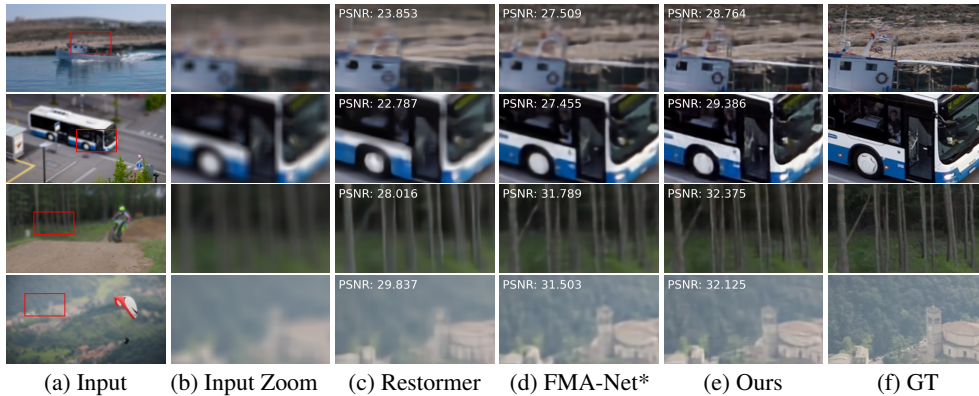


Figure 3: Qualitative examples from the DAVIS-Blur test set demonstrating the fine details preserved by our approach. Superscript (*) indicates models that have been retrained to remove focal blur using our training approach.

5.1 Comparison

Qualitative Evaluation. Visual samples of our model’s outputs on DAVIS-Blur are shown in Figure 3. It can be observed that the DaBiT outputs are considerably more detailed than those from other methods. Additionally, our model shows promise on low-light defocus blur, as tested on select scenes from the BVI-Lowlight dataset [2], shown in Figure 4. In this case, we create a similar test

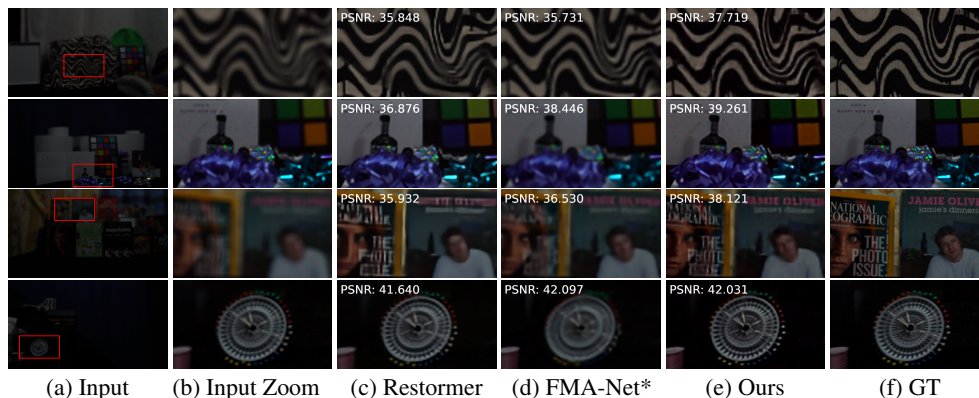


Figure 4: Qualitative examples from blurred BVI-Lowlight scenes showing the performance of our approach on lowlight data. The brightness has been increased by a factor of two for columns (b)–(f) for better visibility. Superscript (*) indicates models that have been retrained to remove focal blur using our training approach.

Approach	Model	PSNR \uparrow	SSIM \uparrow	tOF \downarrow	#P	RT
Video Inpainting	ProPainter [49]	17.962	0.597	4.992	39.4	0.107
Video SR	BasicVSR++ (120p) [5]	25.186	0.679	3.983	7.3	0.022
	BasicVSR++ [5]	25.618	0.713	3.716	7.3	0.150
Image Refocusing	Restormer [45]	24.715	0.698	2.902	26.5	0.093
	APL [47]	23.870	0.605	4.768	13.5	0.017
Joint Refocusing	FMA-Net* [43]	25.691	<u>0.721</u>	2.396	9.6	0.543
	FMA-Net (120p)* [43]	<u>26.860</u>	0.720	<u>2.291</u>	9.6	0.151
	DaBiT (Ours)	28.777	0.811	1.239	45.5	0.112

Table 1: Quantitative comparison results for DaBiT and three other tested methods. For each column, the best result is bold in red and the second best is underlined in blue. The average runtime (RT) for refocusing a 240p frame as well as the number of model parameters (#P) for each method are also reported. For super-resolution models, the output is downsampled to match the 480p ground truth DAVIS scene, and for non-super-resolution models the ground truth is downsampled. Superscript (*) indicates models have been retrained using our defocus blur training approach.

environment to that of DAVIS-Blur, with an initial focal point $f = 0$, a maximum blur kernel of 7×7 , and a focal range of 100.

Quantitative Evaluation. We quantitatively compare our method against several state-of-the-art methods in Table 1. For a fair comparison, deblurring methods not originally designed for removing defocus blur are finetuned using our training approach for 35 epochs. Due to the $4\times$ upscaling nature of FMA-Net and BasicVSR++, we run the models in two ways. In the first, we pass a 240p frame and downsample the output to match the ground truth, and in the second we pass a 120p frame for comparison to the 480p ground truth. The PSNR, SSIM, and tOF are reported for each scenario.

5.2 Ablation Study

Blur Maps and Propagation. To demonstrate the importance of both blur maps and image propagation in our model, we conduct an ablation study with these components removed. Since the image propagation module is not learned, and simply updates the masks and blurry inputs, our model does not need to be retrained. The same is true for the way in which we ablate the blur map by replacing the variable with a tensor of all ones. This is essentially telling the model that the entirety of every frame is blurred, preventing the use of learned performance from blur maps.

Experiment	PSNR \uparrow	SSIM \uparrow	tOF \downarrow
w/o Image Propagation or Blur Maps	25.227	0.703	2.548
w/o Blur Maps	25.311	0.706	2.499
w/o Image Propagation	27.203	0.758	1.914
DaBiT (Ours)	28.777	0.811	1.239

Table 2: Ablation study on the effectiveness of image propagation and the use of blur maps on DAVIS-Blur.

As shown in Table 2, the propagation components benefit our model, but less so than the blur maps. Additionally, the model with neither image propagation nor blur maps exhibits a somewhat surprising tOF score - similar to the model without blur maps. This is likely due to the inability of the model to remove the blur present in the video, since a high degree of blur inherently improves temporal consistency.

6 Conclusion

This paper presents a novel approach to the relatively understudied problem of video focal deblurring. Our method utilises a novel transformer and flow refocusing module, along with bidirectional image propagation, to remove focus blur from a given video sequence. We overcome the limitations of computational resources and speed by working with low-resolution inputs and embedding a super-resolution module in the pipeline. Additionally, we propose a new method to generate synthetic focal blur data, enabling the model to learn from a broader range of content. When compared to other joint video deblurring and super-resolution models on the proposed DAVIS-Blur test set, state-of-the-art performance is achieved. In addition, our model exhibits excellent performance on low-light footage, which often encounters focusing issues. Future work will focus on generalising this approach to other forms of blur, increasing the super-resolution scaling, and investigating if similar performance can be achieved at increased speed by a smaller model using model compression.

7 Acknowledgements

This work was jointly funded by the UK EPSRC (iCASE Award), the BBC, the UKRI MyWorld Strength in Places Programme, and the University of Bristol.

References

- [1] Abdullah Abuolaim and Michael S Brown. “Defocus deblurring using dual-pixel data”. In: *Computer Vision—ECCV 2020: 16th European Conference, Glasgow, UK, August 23–28, 2020, Proceedings, Part X 16*. Springer, 2020, pp. 111–126.
- [2] Nantheera Anantrasirichai et al. “BVI-Lowlight: Fully Registered Benchmark Dataset for Low-Light Video Enhancement”. In: *arXiv preprint arXiv:2402.01970* (2024).
- [3] Shariq Farooq Bhat et al. “Zoedepth: Zero-shot transfer by combining relative and metric depth”. In: *arXiv preprint arXiv:2302.12288* (2023).
- [4] Kelvin CK Chan et al. “Basicvsr: The search for essential components in video super-resolution and beyond”. In: *Proceedings of the IEEE/CVF conference on computer vision and pattern recognition*. 2021, pp. 4947–4956.
- [5] Kelvin CK Chan et al. “Basicvsr++: Improving video super-resolution with enhanced propagation and alignment”. In: *Proceedings of the IEEE/CVF conference on computer vision and pattern recognition*. 2022, pp. 5972–5981.
- [6] Liangyu Chen et al. “Simple Baselines for Image Restoration”. In: *arXiv preprint arXiv:2204.04676* (2022).
- [7] Xuhai Chen et al. “Better” CMOS” Produces Clearer Images: Learning Space-Variant Blur Estimation for Blind Image Super-Resolution”. In: *Proceedings of the IEEE/CVF Conference on Computer Vision and Pattern Recognition*. 2023, pp. 1651–1661.

- [8] Mengyu Chu et al. “Learning temporal coherence via self-supervision for GAN-based video generation”. In: *ACM Transactions on Graphics (TOG)* 39.4 (2020), pp. 75–1.
- [9] Yuning Cui et al. “Image Restoration via Frequency Selection”. In: *IEEE Transactions on Pattern Analysis and Machine Intelligence* (2023).
- [10] Jifeng Dai et al. “Deformable convolutional networks”. In: *Proceedings of the IEEE international conference on computer vision*. 2017, pp. 764–773.
- [11] Alexey Dosovitskiy et al. “An image is worth 16x16 words: Transformers for image recognition at scale”. In: *arXiv preprint arXiv:2010.11929* (2020).
- [12] Akshay Dudhane et al. “Burst Image Restoration and Enhancement”. In: *CVPR*. 2022.
- [13] Chen Gao et al. “Flow-edge guided video completion”. In: *Computer Vision–ECCV 2020: 16th European Conference, Glasgow, UK, August 23–28, 2020, Proceedings, Part XII 16*. Springer. 2020, pp. 713–729.
- [14] Yan Huang, Wei Wang, and Liang Wang. “Bidirectional recurrent convolutional networks for multi-frame super-resolution”. In: *Advances in neural information processing systems* 28 (2015).
- [15] Tae Hyun Kim and Kyoung Mu Lee. “Generalized video deblurring for dynamic scenes”. In: *Proceedings of the IEEE Conference on Computer Vision and Pattern Recognition*. 2015, pp. 5426–5434.
- [16] Meiguang Jin, Givi Meishvili, and Paolo Favaro. “Learning to extract a video sequence from a single motion-blurred image”. In: *Proceedings of the IEEE Conference on Computer Vision and Pattern Recognition*. 2018, pp. 6334–6342.
- [17] Younghyun Jo et al. “Deep video super-resolution network using dynamic upsampling filters without explicit motion compensation”. In: *Proceedings of the IEEE conference on computer vision and pattern recognition*. 2018, pp. 3224–3232.
- [18] Tae Hyun Kim, Seungjun Nah, and Kyoung Mu Lee. “Dynamic video deblurring using a locally adaptive blur model”. In: *IEEE transactions on pattern analysis and machine intelligence* 40.10 (2017), pp. 2374–2387.
- [19] Diederik P Kingma and Jimmy Ba. “Adam: A method for stochastic optimization”. In: *arXiv preprint arXiv:1412.6980* (2014).
- [20] Lingshun Kong et al. “Efficient frequency domain-based transformers for high-quality image deblurring”. In: *Proceedings of the IEEE/CVF Conference on Computer Vision and Pattern Recognition*. 2023, pp. 5886–5895.
- [21] Orest Kupyn et al. “Deblurgan-v2: Deblurring (orders-of-magnitude) faster and better”. In: *Proceedings of the IEEE/CVF international conference on computer vision*. 2019, pp. 8878–8887.
- [22] Dasong Li et al. “A simple baseline for video restoration with grouped spatial-temporal shift”. In: *Proceedings of the IEEE/CVF Conference on Computer Vision and Pattern Recognition*. 2023, pp. 9822–9832.
- [23] Wenbo Li et al. “Mucan: Multi-correspondence aggregation network for video super-resolution”. In: *Computer Vision–ECCV 2020: 16th European Conference, Glasgow, UK, August 23–28, 2020, Proceedings, Part X 16*. Springer. 2020, pp. 335–351.
- [24] Zhen Li et al. “Towards an end-to-end framework for flow-guided video inpainting”. In: *Proceedings of the IEEE/CVF conference on computer vision and pattern recognition*. 2022, pp. 17562–17571.
- [25] Jingyun Liang et al. “Recurrent video restoration transformer with guided deformable attention”. In: *Advances in Neural Information Processing Systems* 35 (2022), pp. 378–393.
- [26] Jingyun Liang et al. “Vrt: A video restoration transformer”. In: *IEEE Transactions on Image Processing* (2024).
- [27] Chengxu Liu et al. “Learning trajectory-aware transformer for video super-resolution”. In: *Proceedings of the IEEE/CVF conference on computer vision and pattern recognition*. 2022, pp. 5687–5696.
- [28] Rui Liu et al. “Fuseformer: Fusing fine-grained information in transformers for video inpainting”. In: *Proceedings of the IEEE/CVF international conference on computer vision*. 2021, pp. 14040–14049.

- [29] Di Ma, Fan Zhang, and David Bull. “BVI-DVC: A Training Database for Deep Video Compression”. In: *IEEE Transactions on Multimedia* (2021), pp. 1–1. DOI: 10.1109/TMM.2021.3108943.
- [30] Federico Perazzi et al. “A benchmark dataset and evaluation methodology for video object segmentation”. In: *Proceedings of the IEEE conference on computer vision and pattern recognition*. 2016, pp. 724–732.
- [31] René Ranftl et al. *Towards Robust Monocular Depth Estimation: Mixing Datasets for Zero-shot Cross-dataset Transfer*. arXiv:1907.01341 [cs]. Aug. 2020. URL: <http://arxiv.org/abs/1907.01341> (visited on 12/28/2023).
- [32] Lingyan Ruan et al. “Learning to deblur using light field generated and real defocus images”. In: *Proceedings of the IEEE/CVF Conference on Computer Vision and Pattern Recognition*. 2022, pp. 16304–16313.
- [33] Wei Shang et al. “Joint Video Multi-Frame Interpolation and Deblurring under Unknown Exposure Time”. In: *Proceedings of the IEEE/CVF Conference on Computer Vision and Pattern Recognition*. 2023, pp. 13935–13944.
- [34] Hyeonseoek Son et al. “Single image defocus deblurring using kernel-sharing parallel atrous convolutions”. In: *Proceedings of the IEEE/CVF International Conference on Computer Vision*. 2021, pp. 2642–2650.
- [35] Zachary Teed and Jia Deng. “Raft: Recurrent all-pairs field transforms for optical flow”. In: *Computer Vision—ECCV 2020: 16th European Conference, Glasgow, UK, August 23–28, 2020, Proceedings, Part II 16*. Springer. 2020, pp. 402–419.
- [36] Yapeng Tian et al. “Tdan: Temporally-deformable alignment network for video super-resolution”. In: *Proceedings of the IEEE/CVF conference on computer vision and pattern recognition*. 2020, pp. 3360–3369.
- [37] Fu-Jen Tsai et al. “Stripformer: Strip transformer for fast image deblurring”. In: *European Conference on Computer Vision*. Springer. 2022, pp. 146–162.
- [38] Zhou Wang et al. “Image quality assessment: from error visibility to structural similarity”. In: *IEEE transactions on image processing* 13.4 (2004), pp. 600–612.
- [39] Ning Xu et al. “Youtube-vos: Sequence-to-sequence video object segmentation”. In: *Proceedings of the European conference on computer vision (ECCV)*. 2018, pp. 585–601.
- [40] Rui Xu et al. “Deep flow-guided video inpainting”. In: *Proceedings of the IEEE/CVF Conference on Computer Vision and Pattern Recognition*. 2019, pp. 3723–3732.
- [41] Yiran Xu et al. “VideoGigaGAN: Towards Detail-rich Video Super-Resolution”. In: (2024). arXiv: 2404.12388 [cs.CV].
- [42] Lihe Yang et al. “Depth Anything: Unleashing the Power of Large-Scale Unlabeled Data”. In: *arXiv:2401.10891* (2024).
- [43] Geunhyuk Youk, Jihyong Oh, and Munchurl Kim. “FMA-Net: Flow-Guided Dynamic Filtering and Iterative Feature Refinement with Multi-Attention for Joint Video Super-Resolution and Deblurring”. In: *arXiv preprint arXiv:2401.03707* (2024).
- [44] Syed Waqas Zamir et al. “Multi-stage progressive image restoration”. In: *Proceedings of the IEEE/CVF conference on computer vision and pattern recognition*. 2021, pp. 14821–14831.
- [45] Syed Waqas Zamir et al. “Restormer: Efficient transformer for high-resolution image restoration”. In: *Proceedings of the IEEE/CVF conference on computer vision and pattern recognition*. 2022, pp. 5728–5739.
- [46] Kaidong Zhang, Jingjing Fu, and Dong Liu. “Flow-guided transformer for video inpainting”. In: *European Conference on Computer Vision*. Springer. 2022, pp. 74–90.
- [47] Wenda Zhao et al. “United defocus blur detection and deblurring via adversarial promoting learning”. In: *European Conference on Computer Vision*. Springer. 2022, pp. 569–586.
- [48] Zhihang Zhong et al. “Blur interpolation transformer for real-world motion from blur”. In: *Proceedings of the IEEE/CVF Conference on Computer Vision and Pattern Recognition*. 2023, pp. 5713–5723.
- [49] Shangchen Zhou et al. “ProPainter: Improving propagation and transformer for video inpainting”. In: *Proceedings of the IEEE/CVF International Conference on Computer Vision*. 2023, pp. 10477–10486.
- [50] Shangchen Zhou et al. “Upscale-A-Video: Temporal-Consistent Diffusion Model for Real-World Video Super-Resolution”. In: *arXiv preprint arXiv:2312.06640* (2023).

- [51] Xizhou Zhu et al. “Deformable convnets v2: More deformable, better results”. In: *Proceedings of the IEEE/CVF conference on computer vision and pattern recognition*. 2019, pp. 9308–9316.

A Appendix 1

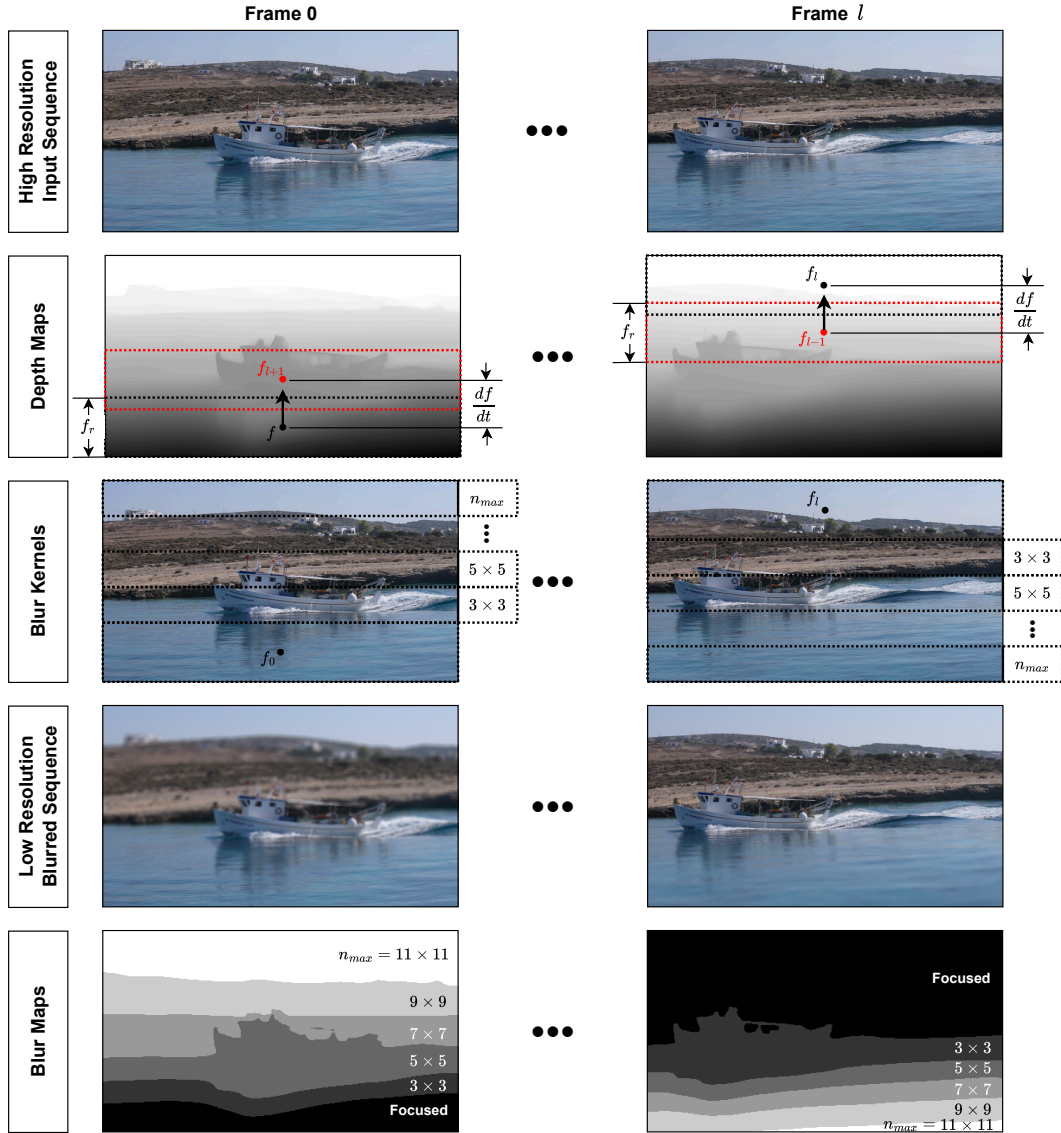


Figure 5: The blurring procedure adopted during training.

Figure 5 shows the blurring process we employ during the training of our model. A high resolution input sequence of length l is selected along with the corresponding depth maps. A random focal point f and focal range f_r are chosen, as well as a random focus rate $\frac{df}{dt}$ and maximum blur size n_{max} . These parameters define a focus shift's size, intensity, and speed, and the focus shifts in the direction it has furthest to travel; in this case, away from the camera. The unfocused area is blurred according to its distance from the focal range; nearer areas are blurred less, and the furthest distances are blurred at the maximum blur size, n_{max} . Note that the rectangular blur regions are an approximation, and the actual regions of the blur at each depth are shown in the generated ground-truth depth map. Finally, we downsample the blurred sequence, along with its blur and depth maps, to obtain a blurred input for training.